Mott Transition and Spin Structures of Spin-1 Bosons in Two-Dimensional Optical Lattice at Unit Filling

Yuta TOGA*, Hiroki TSUCHIURA, Makoto YAMASHITA[1,2], Kensuke INABA[1,2], and Hisatoshi YOKOYAMA[3]

Department of Applied Physics, Tohoku University, Sendai 980-8579, Japan
[1]*NTT Basic Research Laboratories, NTT Corporation, Atsugi, Kanagawa 243-0198, Japan*
[2]*Japan Science and Technology Agency, CREST, Chiyoda, Tokyo 102-0075, Japan*
[3]*Department of Physics, Tohoku University, Sendai 980-8578, Japan*

We study the ground state properties of spin-1 bosons in a two-dimensional optical lattice, by applying a variational Monte Carlo method to the $S = 1$ Bose-Hubbard model on a square lattice at unit filling. A doublon-holon binding factor introduced in the trial state provides a noticeable improvement in the variational energy over the conventional Gutzwiller wave function and allows us to deal effectively with the inter-site correlations of particle densities and spins. We systematically show how spin-dependent interactions modify the superfluid-Mott insulator transitions in the $S = 1$ Bose-Hubbard model due to the interplay between the density and spin fluctuations of bosons. Furthermore, regarding the magnetic phases in the Mott region, the calculated spin structure factor elucidates the emergence of nematic and ferromagnetic spin orders for antiferromagnetic ($U_2 > 0$) and ferromagnetic ($U_2 < 0$) couplings, respectively.

KEYWORDS: Mott transition, superfluid, insulating state, nematic phase, ferromagnetism, $S = 1$ Bose-Hubbard model, doublon-holon binding, variational Monte Carlo method

Recent progress in ultracold atom experiments has offered unprecedented opportunities for exploring fundamental quantum phenomena in strongly correlated many-body systems that have been largely ignored in conventional condensed-matter physics. A prominent example of such phenomena is the quantum phase transition from a superfluid (SF) to a Mott insulator (MI), demonstrated using cold bosons with frozen spin degrees of freedom trapped in optical lattices.[1)] Furthermore, quantum gas microscope techniques[2–5)] have opened the door to the detection and manipulation of single bosons at a single site level in an optical lattice, just like scanning tunneling microscopy in solid state physics. Quite recently, Endres *et al.*[6)] used this technique to track the SF-MI transition in more detail, and found that correlated pairs consisting of a doubly populated site (doublon, D) and an unpopulated site (holon, H), which represent the excitations in an MI, fundamentally determine the properties of the SF-MI transition, which is consistent with recent numerical studies.[7,8)]

Now theoretical interest is naturally moving towards the quantum phase transitions in bosons with *unfrozen* spin degrees of freedom[9,10)] trapped in optical lattices. The doublon, which is one fragment of the elementary excitation in an MI, will have internal spin structures unlike spinless (spin-frozen) systems. Thus, we can strongly expect the interplay between spin correlations and the SF-MI transition to play key roles in the ground state of the systems. The simplest of such systems will be $S = 1$ bosons on an optical lattice, whose properties are well captured by the $S = 1$ Bose-Hubbard model (BHM)[11)]

$$\mathcal{H} = -t \sum_{\langle i,j \rangle} \sum_{\alpha} \left(\hat{a}^{\dagger}_{i,\alpha} \hat{a}_{j,\alpha} + \hat{a}^{\dagger}_{j,\alpha} \hat{a}_{i,\alpha} \right) - \mu \sum_{i} \hat{n}_i + \frac{U_0}{2} \sum_{i} \hat{n}_i (\hat{n}_i - 1) + \frac{U_2}{2} \sum_{i} \left(\hat{\boldsymbol{S}}^2_i - 2\hat{n}_i \right), \quad (1)$$

where $a_{j,\alpha}$ is an annihilation operator of a boson of spin α at the site j, $\hat{n}_j = \sum_{\alpha} \hat{a}^{\dagger}_{j,\alpha} \hat{a}_{j,\alpha}$ and $t, U_0 > 0$. Here, $\alpha = -1, 0, 1$, and $\langle i, j \rangle$ denotes a nearest-neighbor-site pair; the definition of t is a half of that reported in some studies. The spin-dependent (last) term in eq. (1) induces spin mixing and enriches the physics of this model, compared with spinless models. In cold-atom systems, the values of U_0 and U_2 depend on the s-wave scattering wavelength characteristic of the atom species; $U_2 > 0$ (< 0) for Na (Rb) atoms. In contrast to more familiar Fermi-Hubbard models with $S = 1/2$ where an antiferromagnetic superexchange interaction prevails in the strongly correlated regime, the $S = 1$ BHM exhibits complicated effective inter-site spin interactions that lead to exotic magnetic phases,[12,13)] owing to the absence of the Pauli exclusion principle. Thus far, the phase diagram of this model has been studied based on mean-field type theories[14,15)] including a Gutzwiller approximation (GA),[16,17)] and on density matrix renormalization group[18,19)] and quantum Monte Carlo (QMC) methods for the one-dimensional system.[20,21)] Alternatively, at the cost of the density fluctuation, an effective spin Hamiltonian obtained by a strong-coupling expansion[12,15,22)] was studied to explore the magnetic structures in the MI phase using QMC calculations in two and three dimensions.[23)]

In this letter, we provide a consistent description of the ground state properties and the phase transition from SF to MI of the $S = 1$ BHM on a square lattice, focusing on correlated pair excitations based on a variational Monte Carlo (VMC) approach, which is beyond conventional mean-field and GA techniques. We consider the simplest

*E-mail address: toga@solid.apph.tohoku.ac.jp

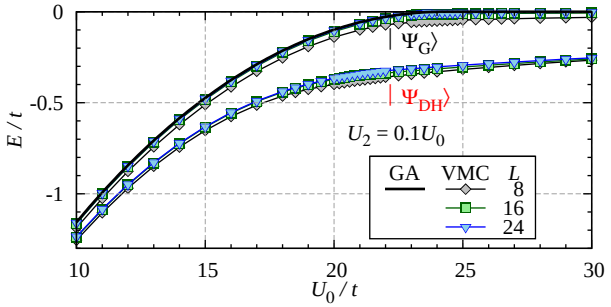

Fig. 1. (Color online) The total energy per site of $|\Psi_{\rm G}\rangle$ and $|\Psi_{\rm DH}\rangle$ is compared as a function of U_0/t for three system sizes. The VMC data of $|\Psi_{\rm G}\rangle$ for finite L's will converge to the GA result, the exact analytic result of $|\Psi_{\rm G}\rangle$ for $L=\infty$. The ratio U_2/U_0 is fixed at 0.1, and the result is similar to that of $U_2=0$.

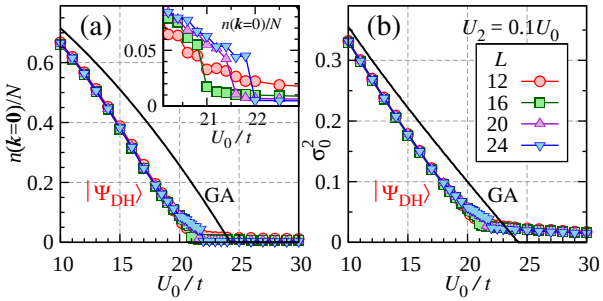

Fig. 2. (Color online) (a) Condensate fraction or momentum distribution function at $\boldsymbol{k}=(0,0)$ and (b) density fluctuation, as a function of U_0/t for $|\Psi_{\rm G}\rangle$ and of $|\Psi_{\rm DH}\rangle$ for $U_2/U_0=0.1$. The inset in (a) shows an enlarged view near the Mott transition point.

case of an SF-MI transition so that we restrict the particle density $\rho=N/N_s$ (N: particle number, N_s: the total number of sites) to $\rho=1$ (unit filling) and put $\mu=0$. We consider the behavior for other odd commensurate densities ($\rho=3,5,\cdots$) to be essentially the same. We will report even-ρ cases separately.

To implement VMC calculations, we employ an occupation number representation at each site, $|n_1,n_0,n_{-1}\rangle$. As a variational wave function, we use a Jastrow-type, $|\Psi_{\rm DH}\rangle = \mathcal{P}_{\rm DH}\mathcal{P}_{\rm G}|\Phi\rangle$. Here $|\Phi\rangle$ is the one-body part: $|\Phi\rangle = \frac{1}{\sqrt{N_s!}}\left(\hat{a}^\dagger_{\boldsymbol{0},1}+\hat{a}^\dagger_{\boldsymbol{0},0}+\hat{a}^\dagger_{\boldsymbol{0},-1}\right)^{N_s}|0\rangle$, where, $\hat{a}^\dagger_{\boldsymbol{0},1}$ indicates the $\boldsymbol{k}=\boldsymbol{0}$ component of the Fourier transformation of $\hat{a}^\dagger_{j,1}$. Since the total S_z is well conserved in cold atom systems, we work in the subspace of $\sum_j S^z_j=0$. As an onsite correlation factor, the Gutzwiller projection is extended so that it depends on the spin configurations in the site,[17]

$$\mathcal{P}_{\rm G}=\prod_j \gamma(n_{j,1},n_{j,0},n_{j,-1})|n_1,n_0,n_{-1}\rangle_j\ {}_j\langle n_1,n_0,n_{-1}|, \tag{2}$$

where coefficients γ are variational parameters controlling $n_{j,\alpha}$, the occupation particle number of spin α on the site j. The dependence on spin configuration is necessary for $U_2\neq 0$. Since we have confirmed that the probability $P(n)$ for $n\geq 4$ becomes negligible for the value of interest, $U_0/t\gtrsim 10$, we impose a restriction, $\gamma(n_{j,1},n_{j,0},n_{j,-1})=0$, on the total occupation number (n) at each site for $n_j\equiv n_{j,1}+n_{j,0}+n_{j,-1}\geq 4$. The D-H correlation factor $\mathcal{P}_{\rm DH}(\eta,\eta\prime)$ used here is the same as that introduced in refs. 7 and 8, where η (η') is a variational parameter ($0\leq\eta\leq 1$) that controls the strength of the D-H binding between nearest-neighbor (lattice-diagonal) sites. For $\eta=1$, isolated doublons and holons are prohibited. We assume η and η' are independent of the onsite spin configuration for simplicity. It should be noted here that in effect a multiply populated site means a doublon for $U_0/t\gtrsim 20$, because $P(n)$ for $n\geq 3$ almost vanishes.

In the VMC calculations, we first optimized the variational parameters using a quasi-Newton method, and calculated the quantities for sets of model parameters (U_0/t, U_2/t) with several million configurations for several system sizes of $N_s=L\times L$ sites with $L=$ 8-24.

We start by discussing the features of a Mott transition in $|\Psi_{\rm DH}\rangle$ by comparing those obtained with a Gutzwiller wave function $|\Psi_{\rm G}\rangle=\mathcal{P}_{\rm G}|\Phi\rangle$ when the ratio U_2/U_0 is fixed at 0.1. Figure 1 shows how the total energy E/t is improved by employing $|\Psi_{\rm DH}\rangle$ in the region of intermediate correlation strength. The value of $|\Psi_{\rm G}\rangle$ arrives at zero at the Brinkman-Rice transition point,[24] $U_0^{\rm BR}/t\sim 24.3$. On the other hand, E/t of $|\Psi_{\rm DH}\rangle$ is considerably less than that of GA, and remains finite even for large U_0/t values.

In Fig. 2(a), the condensate fraction or $\boldsymbol{k}=(0,0)$ element of the momentum distribution function, $n(\boldsymbol{k})=\sum_\alpha\langle\hat{a}^\dagger_{\boldsymbol{k},\alpha}\hat{a}_{\boldsymbol{k},\alpha}\rangle$, is plotted as a function of U_0/t. This quantity is finite in the SF phase, but should vanish as $1/N_{\rm s}$ in the MI phase. The value of $|\Psi_{\rm DH}\rangle$ exhibits a sudden drop (for $L\geq 16$) at $U_0=U_{0\rm c}\sim 22t$ and vanishes as $1/N_{\rm s}$ for $U_0>U_{0\rm c}$ in the inset shown in Fig. 2(a). $n(\boldsymbol{k}=\boldsymbol{0})/N$ is regarded as an order parameter of the Mott transition here, and so this anomaly indicates a first-order SF-MI transition. In fact, we confirmed that the small-$|\boldsymbol{q}|$ behavior of the density correlation function $N(\boldsymbol{q})$ (not shown) changes suddenly from linear to quadratic in momentum $|\boldsymbol{q}|$ at $U_0=U_{0\rm c}$. These features are substantially identical to those in the spinless case on the same D-H binding mechanism.[8] Next, let us look at the density fluctuation, $\sigma_0^2=\langle\hat{n}^2\rangle-\langle\hat{n}\rangle^2$, which is shown in Fig. 2(b). As is known, the σ_0^2 of GA completely vanishes at $U_0=U_0^{\rm BR}$, which corroborates the view that each site is occupied by exactly one particle in the MI phase. On the other hand, σ_0^2 of $|\Psi_{\rm DH}\rangle$ exhibits a small step at $U_0=U_{0\rm c}$ and remains finite for $U_0>U_{0\rm c}$. This finite density fluctuation is reflected in the small but finite values of $P(0)\sim P(2)$. In the following, we show that the doublon plays a crucial role for the spin structure.

Now, we turn to the spin-dependent features caused by the U_2-term in $\mathcal{H}$. In Fig. 3(a), the optimized values of the D-H binding parameter η are plotted to recognize the effects of the U_2-term on the SF-MI transition. Recall that η controls the strength of the D-H binding between nearest-neighbor sites, and $\eta=1$ means that each doublon is tightly bound to an adjacent holon. We find that the SF-MI transition point $U_{0\rm c}/t$ shifts to noticeably larger values for $U_2/U_0=0.3$ and -0.1, whereas the shift for $U_2/U_0=0.1$ is very small.

First, let us consider the difference in the U_{0c} shift between for $U_2/U_0=\pm 0.1$. Since the system is in the vicinity of the MI phase ($U_0\gg t$), we may restrict the Fock space to $n_j=0,1,2$ at each site; actually we confirmed

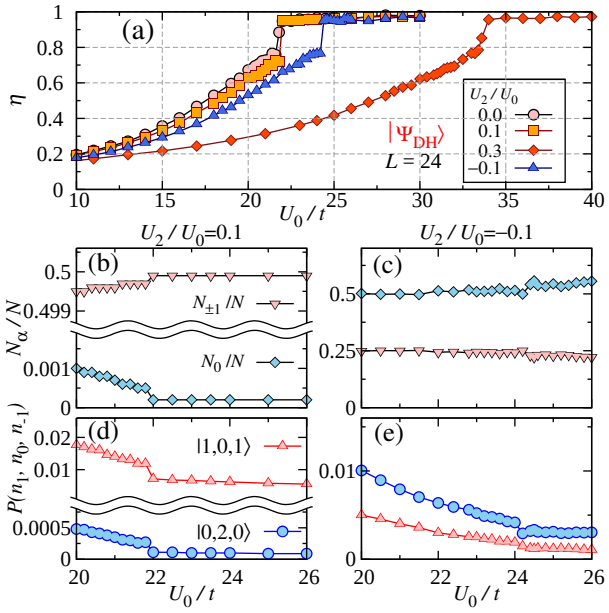

Fig. 3. (Color online) (a) U_2/U_0 dependence of optimized D-H binding parameter η as a function of U_0/t. (b),(c) show the number fraction of atoms with each spin-component and (d),(e) show the probabilities of doublons with each spin state around U_{0c}/t for $U_2/U_0 = \pm 0.1$.

that $n_j \geq 3$ is negligible for $U_0/t \gtrsim 20$. To minimize the ground state energy for $U_2 \neq 0$, not only the number of doubly populated ($n = 2$) sites but also their spin structures have to be optimized. To this end, it is convenient to employ the eigenstates of $\hat{\boldsymbol{S}}_j^2$, $|S_j, S_j^z\rangle\rangle$, where S_j and S_j^z indicate the magnitude and z-component of the total spin at the site-j, respectively; S_j is even (odd) when an even (odd) number of atoms occupy the site-j. Using $|S_j, S_j^z\rangle\rangle$, our basis set $|n_{j,1}, n_{j,0}, n_{j,-1}\rangle$ for $n = 2$ is represented as

$$
\begin{aligned}
|2,0,0\rangle &= |2,2\rangle\rangle, \quad |1,1,0\rangle = |2,1\rangle\rangle, \\
|0,2,0\rangle &= \frac{1}{\sqrt{3}}\left(\sqrt{2}|2,0\rangle\rangle + |0,0\rangle\rangle\right), \\
|1,0,1\rangle &= \frac{1}{\sqrt{3}}\left(|2,0\rangle\rangle - \sqrt{2}|0,0\rangle\rangle\right). \qquad (3)
\end{aligned}
$$

According to eq. (3), the on-site energies of $n = 2$ sites are calculated as $U_0 + U_2$ for $|2,0,0\rangle$ and $|1,1,0\rangle$, U_0 for $|0,2,0\rangle$, and $U_0 - U_2$ for $|1,0,1\rangle$. We also define the probability $p_\alpha = N_\alpha/N_s$ ($\alpha = -1, 0, 1$), where N_α denotes the total number of particles of spin α; in the present case, p_α obeys the conditions $0 \leq p_\alpha \leq 1$ and $\sum_\alpha p_\alpha = 1$. Since we assume $\sum_j S_j^z = 0$, the relation $p_1 = p_{-1}$ holds, resulting in $2p_1 + p_0 = 1$. Using these formulae, the classical statistical weights for the $n = 2$ configurations can be calculated as $(p_1)^2$ for $|2,0,0\rangle$, $2(p_1)^2$ for $|1,0,1\rangle$, $(p_0)^2$ for $|0,2,0\rangle$, and $2p_0p_1$ for $|1,1,0\rangle$. For $U_2 \sim t$, the expectation value of the U_2-term per site is similarly obtained as

$$
E_2(p_1) \propto -U_2 p_1 \left(p_1 - 1/2\right). \qquad (4)
$$

This energy has the minimum value $U_2/2$ at $p_1 = 1/4$ for $U_2 < 0$, and 0 at $p_1 = 0$ and $1/2$ for $U_2 > 0$. Actually, the VMC results in Figs. 3(b) and 3(c) show $p_1 = N_1/N_s \simeq 1/4$ for $U_2/U_0 = -0.1$, and $p_1 \simeq 0.5$ for $U_2/U_0 = 0.1$. This causes imbalanced spin population for $n = 2$ sites, as shown in Figs. 3(d) and 3(e). Thus, we find through eq. (4) that the on-site energies of $n = 2$ sites are renormalized to $U_0 + U_2/2$ for $U_2 < 0$, while they are not renormalized for $U_2 > 0$. Since the onsite energies of $n = 2$ sites primarily govern the SF-MI transition, this is an appropriate explanation of the difference in the U_{0c}/t shifts between for $U_2/U_0 = \pm 0.1$. Finally, we point out that the degeneracy in U_2-energy between $p_1 = 0$ and 0.5 for $U_2 > 0$ found in eq. (4) is owing to the present spin-1 rotational symmetry, namely, $|S^x = 0\rangle = (|S^z = 1\rangle + |S^z = -1\rangle)/\sqrt{2}$. Therefore, we can generate a ground state with $p_1 \simeq 0$ using VMC if we choose a certain initial condition with $p_0 \gg p_1$.

Next, we discuss the difference in the U_{0c}/t shifts between for $U_2/U_0 = 0.1$ and 0.3. In the above discussion, we adopted a *classical* statistical weighting [E_2 in eq. (4)], which ignores the effect of spin fluctuation caused by the U_2-term, because the spin fluctuation (or singlet formation) is suppressed by the particle hopping for small $|U_2|/U_0$'s. This is not the case for large $|U_2|/U_0$'s. When the U_2-term becomes predominant over the hopping term, the singlet state $|0,0\rangle\rangle = 1/\sqrt{3}\left(|0,2,0\rangle - \sqrt{2}|1,0,1\rangle\right)$ becomes significant in $n = 2$ sites, in order to reduce further the U_2-energy through the spin-exchange processes in the $\hat{\boldsymbol{S}}^2$-term. In this case, assuming $U_2 \gg t$, we ignore the hopping term and directly diagonalize the interaction part in $\mathcal{H}$ using $|S_j, S_j^z\rangle\rangle$. As a result, we find that the on-site energy of $n = 2$ sites is renormalized toward $U_0 - 2U_2$, which vanishes for $U_2/U_0 = 0.5$. Thus, the value of U_{0c}/t is bound to grow rapidly as U_2/U_0 approaches 0.5, which explains the pronounced shift for $U_2/U_0 = 0.3$ in Fig. 3(a).

Now, we study the magnetic structures and the spin correlations in the ground state around the SF-MI transition. For $U_2/U_0 > 0$, the imbalance of the spin populations found in Fig. 3 (d) suggests that the ground state of the system exhibits the spin-nematic property. To detect this with regard to the present case, it is useful to study not only spin-correlation functions but also a spin-nematic parameter Q_α defined as

$$
Q_\alpha = \frac{1}{N_s}\sum_j \left\langle \left(\hat{S}_j^\alpha\right)^2 - \frac{1}{3}\hat{\boldsymbol{S}}_j^2 \right\rangle . \qquad (5)
$$

The maximum value of Q_α for a single atom with $S = 1$ is 1/3, which is realized in, e.g., $|1,0,0\rangle$ and $|0,0,1\rangle$, and also in the eigenstates of $\hat{S}^x$ with $S^x = 0$, which can be expressed as a coherent superposition of $|1,0,0\rangle$ and $|0,0,1\rangle$. Of course, isotropic spin gives $Q_\alpha = 0$. Figure 4 shows Q_z for two positive values of U_2/U_0. Reflecting the imbalanced spin population shown in Fig. 3 (d), large values of Q_z are observed in the whole range of $U_0/t > 0$, that is, both in the SF and MI phases. In the MI phase, the single site state is not a coherent superposition of $|1,0,0\rangle$ and $|0,0,1\rangle$ due to the restriction of $\sum_j S_j^z = 0$. Thus, the spins in the MI phase exhibit a rod-like nematic structure with $Q_z \sim 1/3$ and $Q_x = Q_y \sim -1/6$. Here, as mentioned in the previous paragraph, the population of doublon $|0,2,0\rangle$ and thus N_0 increases as U_2/U_0 increases, which leads to lower Q_z values. This is made

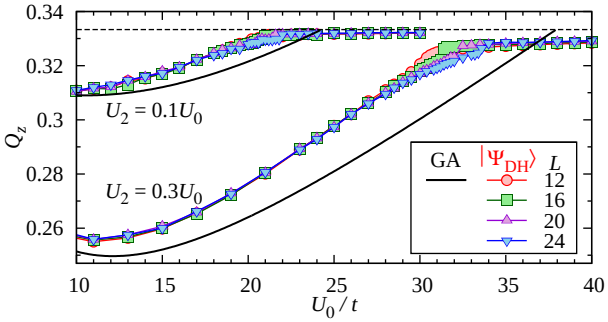

Fig. 4. (Color online) Spin nematic parameter Q_z for two positive values of U_2/U_0. For comparison, the GA result is also plotted, where, in fact, Q_z cannot be determined for $U_0 > U_0^{\rm BR}$.

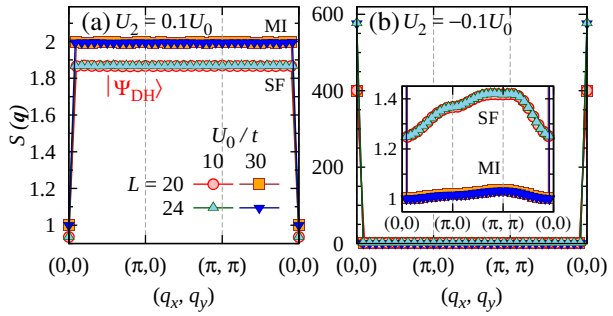

Fig. 5. (Color online) Example of spin structure factor for (a) antiferromagnetic coupling ($U_2 > 0$) and (b) ferromagnetic coupling ($U_2 < 0$). The phase for $U_0/t = 10$ (30) is SF (MI). The inset in (b) shows enlarged views of the two phases.

manifest in that Q_z for $U_2/U_0 = 0.3$ is smaller than that for $U_2/U_0 = 0.1$. The minima of Q_z at $U_0/t \sim 10$ have the same cause, i.e., in the lower U_0 region, Q_z decreases with increase in U_0/t due to an accompanying increase of U_2, but, for $U_0/t \gtrsim 10$, Q_z enhances as U_0/t increases as a result of decrease of doublon density. In the same context, Q_z is slightly reduced from the full-moment value 1/3 in the MI phase, where the D-H factor in $|\Psi_{\rm DH}\rangle$ induces a particle density fluctuation, in contrast to GA. Incidentally, the spin directions remain arbitrary and indefinite for $U_2 = 0$ or $U_0 = 0$, indicating that the point of $U_2/U_0 = 0$ is singular. In addition, we show the spin structure factor, $S(\boldsymbol{q}) = \frac{1}{N_{\rm s}} \sum_{j,\ell} \langle \hat{\boldsymbol{S}}_j \cdot \hat{\boldsymbol{S}}_\ell \rangle e^{i\boldsymbol{q}\cdot\boldsymbol{R}_{j\ell}}$, for $U_2/U_0 = 0.1$ in Fig. 5(a). The constant $S(\boldsymbol{q})$ indicates that there is no spin correlation, and the spins take random directions. Here, the decrease in $S(\boldsymbol{q} = \boldsymbol{0})$ is reflected in the restriction of $\sum_j S_j^z = 0$. Thus, we find a nematic order is realized for $U_2/U_0 > 0$.

For $U_2/U_0 < 0$, Q_z becomes negative and its absolute value decreases monotonically as U_0/t increases for $U_0 < U_{0c}$, and is almost constant $\sim -1/6$ in the MI phase (not shown), indicating that the spins are polarized in the x-y plane. In Fig. 5(b), $S(\boldsymbol{q})$ for $U_2/U_0 = -0.1$ is plotted in the two phases. By considering that the value of $S(\boldsymbol{q} = \boldsymbol{0})$ is extremely large with almost full moment and diverges proportionally to $N_{\rm s}$, a ferromagnetic (FM) long-range order is realized in the x-y plane. The magnitude of the FM moment is almost constant in both the SF and MI phases (not shown but expected from Fig. 5(b)). The results reported above (for $U_2 \gtrless 0$) are consistent with those at the weak- (SF, $t \gg U_0 \gg |U_2|$)[17] and strong- (MI, $t \to 0$)[23] interaction limits.

In summary, the $S = 1$ Bose-Hubbard model [eq. (1)] on a square lattice at unit filling is studied, using a variational Monte Carlo method. A doublon-holon binding factor $\mathcal{P}_{\rm DH}$, which is the essence of Mott transitions, not only improves the variational energy considerably upon the GA, but enables us to study the details of the spin structure directly even in the MI phase without resorting to an effective spin Hamiltonian. For $U_2 > 0$ (< 0), a spin nematic (ferromagnetic) phase is stabilized from SF to MI phases. The present results broadly support the phase diagrams[14–16] and spin structure[17,23] as regards $S = 1$ BHM proposed in previous studies.

Some of the numerical computations were carried out at the Yukawa Institute Computer Facility and at the Cyberscience Center, Tohoku University. This work is supported by a Grant-in-Aid for Scientific Research (C) and also by the Next Generation Supercomputing Project, Nanoscience Program, from MEXT of Japan.

1) M. Greiner, O. Mandel, T. Esslinger, T. W. Hänsch, and I. Bloch: Nature **415**(2002) 39.
2) W. S. Bakr, J. I. Gillen, A. Peng, S. Fölling, and M. Greiner: Nature **462** (2009) 74.
3) W. S. Bakr, A. Peng, M. E. Tai, J. Simon, J. I. Gillen, S. Fölling, L. Pollet, and M. Greiner: Science **329** (2010) 547.
4) J. F. Sherson, C. Weitenberg, M. Endres, M. Cheneau, I. Bloch, and S. Kuhr: Nature **467** (2010) 68.
5) C. Weitenberg, M. Endres, J. F. Sherson, M. Cheneau, P. Schauß, T. Fukuhara, and I. Bloch: Nature **471** (2011) 319.
6) M. Endres, M. Cheneau, T. Fukuhara, C. Weitenberg, P. Schauß, C. Gross, L. Mazza, M. C. Bañuls, L. Pollet, I. Bloch, and S. Kuhr: Science **334** (2011) 200.
7) M. Capello, F. Becca, M. Fabrizio, and S. Sorella: Phys. Rev. Lett. **99** (2007) 056402; Phys. Rev. B **77** (2008) 144517.
8) H. Yokoyama and M. Ogata: J. Phys. Chem. Solids **69** (2008) 3356; H. Yokoyama, T. Miyagawa, and M. Ogata: J. Phys. Soc. Jpn **80** (2011) 084607.
9) T. L. Ho: Phys. Rev. Lett. **81** (1998) 742; T. Ohmi and K. Machida: J. Phys. Soc. Jpn. **67** (1998) 1822; D. M. Stamper-Kurn, M. R. Andrews, A. P. Chikkatur, S. Inouye, H.-J. Miesner, J. Stenger, and W. Ketterle: Phys. Rev. Lett. **80** (1998) 2027.
10) M. Koashi and M. Ueda: Phys. Rev. Lett. **84** (2000) 1066; T. L. Ho and S. K. Yip: Phys. Rev. Lett. **84** (2000) 4031.
11) E. Demler and F. Zhou: Phys. Rev. Lett. **88** (2002) 163001.
12) A. Imambekov, M. Lukin, and E. Demler: Phys. Rev. A **68** (2003) 063602.
13) M. Snoek, and F. Zhou: Phys. Rev. B **69** (2004) 094410.
14) K. V. Krutitsky, and R. Graham: Phys. Rev. A **70** (2004) 063610.
15) S. Tsuchiya, S. Kurihara, and T. Kimura: Phys. Rev. A **70** (2004) 043628.
16) T. Kimura, S. Tsuchiya, and S. Kurihara: Phys. Rev. Lett. **94** (2005) 110403.
17) M. Yamashita and M. W. Jack: Phys. Rev. A **76** (2007) 023606.
18) M. Rizzi, D. Rossini, G. De Chiara, S. Montangero, and R. Fazio: Phys. Rev. Lett. **95** (2005) 240404.
19) S. Bergkvist, I. P. McCulloch, and A. Rosengren: Phys. Rev. A **74** (2006) 053419.
20) V. Apaja and O. F. Syljuåsen: Phys. Rev. A **74** (2006) 035601.
21) G. G. Batrouni, V. G. Rousseau, and R. T. Scalettar: Phys. Rev. Lett. **102** (2009) 140402.
22) S. K. Yip: Phys. Rev. Lett. **90** (2003) 250402.
23) K. Harada and N. Kawashima: Phys. Rev. B **65** (2002) 052403.

24) W. F. Brinkman and T. M. Rice: Phys. Rev. B **2** (1970) 4302.